Spectrochimica Acta Part A: Molecular and Biomolecular Spectroscopy 117 (2014) 234–244

Contents lists available at ScienceDirect

Spectrochimica Acta Part A: Molecular and Biomolecular Spectroscopy

journal homepage: www.elsevier.com/locate/saa

The spectroscopic (FT-IR, FT-Raman, UV and NMR) first order hyperpolarizability and HOMO–LUMO analysis of dansyl chloride

M. Karabacak [a], M. Cinar [b], M. Kurt [c], A. Poiyamozhi [d], N. Sundaraganesan [e,*]

[a] Department of Mechatronics Engineering, H.F.T. Technology Faculty, Celal Bayar University, 45400 Turgutlu, Manisa, Turkey
[b] Department of Science Education, Bayburt University, 69000 Bayburt, Turkey
[c] Department of Physics, Ahi Evran University, 40100 Kırsehir, Turkey
[d] Department of Physics, Government Arts College, Dharmapuri 636 705, India
[e] Department of Physics (Engg.), Annamalai University, Annamalai Nagar, 608 002 Chidambaram, Tamil Nadu, India

HIGHLIGHTS

- The FT-IR and FT-Raman spectra of dansyl chloride were recorded.
- The vibrational frequencies were calculated by DFT method and discussed.
- NMR and UV–Vis spectra were also recorded and compared with calculated ones.

GRAPHICAL ABSTRACT

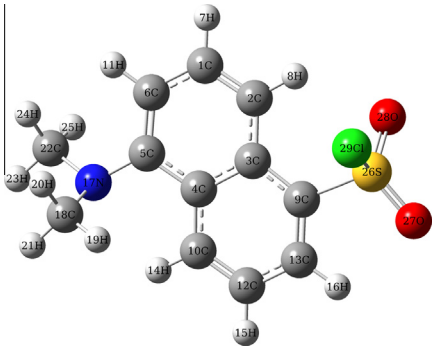

ARTICLE INFO

Article history:
Received 3 July 2012
Accepted 29 July 2013
Available online 7 August 2013

Keywords:
TD-DFT
Vibrational spectra
PES scan analysis
First order hyperpolarizability
NMR
Dansyl chloride

ABSTRACT

The solid phase FT-IR and FT-Raman spectra of dansyl chloride (DC) have been recorded in the regions 400–4000 and 50–4000 cm^{-1}, respectively. The spectra have been interpreted in terms of fundamentals modes, combination and overtone bands. The structure of the molecule has been optimized and the structural characteristics have been determined by density functional theory (B3LYP) method with 6-311++G(d,p) as basis set. The vibrational frequencies were calculated for most stable conformer and were compared with the experimental frequencies, which yield good agreement between observed and calculated frequencies. The infrared and Raman spectra have also been predicted from the calculated intensities. ^{1}H and ^{13}C NMR spectra were recorded and ^{1}H and ^{13}C nuclear magnetic resonance chemical shifts of the molecule were calculated using the gauge independent atomic orbital (GIAO) method. UV–Visible spectrum of the compound was recorded in the region 200–600 nm and the electronic properties HOMO and LUMO energies were measured by time-dependent TD-DFT approach. Nonlinear optical and thermodynamic properties were interpreted. All the calculated results were compared with the available experimental data of the title molecule.

Introduction

In the last few years, many various derivatives of dansyl chloride (5-dimethylamino-1-naphthalenesulfonyl chloride) as a complexing agent have been extensively used in different studies [1–5]. DC is an important and widely used fluorescence reagent, reacting with amino, phenolic and active hydroxyl groups under suitable experimental conditions [6,7]. DC is a yellow crystalline powder that reacts violently with water. Many studies concerning DC have been carried out in the literature [8–13]. DC has been used recently to improve ESI signal intensity [14] and more specifically for ultra trace analysis of ethinyl estradiol in human plasma [15].

* Corresponding author. Tel.: +91 9442068405.
E-mail address: sundaraganesan_n2003@yahoo.co.in (N. Sundaraganesan).

1386-1425/$ - see front matter © 2013 Elsevier B.V. All rights reserved.
http://dx.doi.org/10.1016/j.saa.2013.07.095

Dansyl chloride derivatives are fluorometric detection reagents emitted by UV light, and can be extensively used as a fluorescent label in immunofluorescence methods as well as in yielding fluorescent N-terminal amino acids and peptide derivatives. Dansyl and its derivatives can be applied as synthetic receptors to selectively bind a wide variety of guest molecules/ions forming the host–guest complexes [16,17]. DC can also be dangerous to respiratory system, eyes, skin, and mucous membranes.

Literature survey reveals that to the best of our knowledge, the results based on quantum chemical calculations, vibrational spectral, UV, NMR studies and HOMO–LUMO and MEP analyses on DC molecule have no reports.

Nowadays, quantum chemical calculations have been proven to be an important tool for investigation of the relationships between structures and spectral properties of the organic molecules and for the interpretation of experimental data arising from industrial interest and applications. By means of increasing development of computational chemistry in the past decade, the research of theoretical modeling of drug design, functional material design, etc., has become much more established than ever. Many important chemical and physical properties of biological and chemical systems can be predicted from the first principles by various computational techniques [18,19].

Hence, we desired to originate a spectroscopic characterization of DC molecule with a view to get some insight into structure–function relationship through spectra-structure correlation. In order to achieve this objective, FT-Raman, FT-IR, NMR and UV spectroscopic studies along with HOMO (highest occupied molecular orbital)–LUMO (lowest unoccupied molecular orbital) and MEP analysis have been performed by applying density functional theory calculations based on Becke3-Lee–Yang–Parr (B3LYP) with 6-311++G(d,p) as basis set.

Experimental details

The FT-IR spectrum of DC recorded in the region 400–4000 cm^{-1} on a Perkin Elmer FT-IR BX spectrometer calibrated using polystyrene bands. The FT-Raman spectrum of the sample recorded using 1064 nm line of Nd:YAG laser as excitation wave length in the region 50–4000 cm^{-1} on a Bruker RFS 100/S FT-Raman spectrometer. The detector is a liquid nitrogen cooled Ge detector. Five hundred scans were accumulated at 4 cm^{-1} resolution using a laser power of 100 mW. NMR experiments were performed in Bruker DPX 600 MHz at 300 K. The compound was dissolved in DMSO. Chemical shifts were reported in ppm relative to tetramethylsilane (TMS) for ^{1}H and ^{13}C NMR and DEPT 135 spectra. ^{1}H and ^{13}C NMR spectra were obtained at a base frequency of 600 MHz and 150 MHz, respectively. The ultraviolet absorption spectrum of DC molecule dissolved in water and ethanol are examined in the range 200–600 nm using Shimadzu UV-1800 PC, UV–Vis recording Spectrometer. Data are analyzed by UV PC personal spectroscopy software, version 3.91.

Computational details

All calculations in this paper were executed with the Gaussian 03 program [20]. In the DFT calculations, the B3LYP functional combined with the 6-311++G(d,p) basis set were used for geometry optimization, computation of harmonic vibrational frequencies, calculation of binding energies and excitation energies. All vibrational frequencies were found to be real which indicates that a true minimum on hypersurface of total energy was found. By using Gauss-View molecular visualization program [21], the vibrational bands assignments have been made. The vibrational assignments of the normal modes were made on the basis of the TED calculated results by using the VEDA 4 program [22]. As the hybrid B3LYP functional tends to overestimate the fundamental normal modes of vibration, the computed frequencies were scaled with appropriate values to bring harmonization between theoretical and experimental wavenumbers [23–26]. The wavenumber-linear scaling (WLS) method is a general and simple scaling procedure to correct the calculated harmonic frequencies. The electronic absorption spectra were calculated using the time-dependent density functional theory (TD-DFT) method [27–30]. Also, it is calculated in water and ethanol solution using the Polarizable Continuum Model (PCM) [31–34]. To investigate the reactive sites of the compound the molecular electrostatic potential was evaluated using the DFT method. The linear polarizability and first hyperpolarizability properties of the compound were obtained from molecular polarizabilities based on theoretical calculations.

Results and discussion

Molecular structure

The first task for the computational work is to determine the optimized geometries of the studied molecules. The optimized molecular structure of DC with the numbering scheme of the atoms obtained from Gauss view program [35] is shown in Fig. 1. The optimized structural parameters such as bond lengths, bond angles and dihedral angles of DC are determined by B3LYP method with 6-311++G(d,p) as basis set were compared with experimental parameters obtained from the X-ray data studies [36] shown in Table 1. The longest bond distance C3—C9 (1.435 Å) is due to the fusion of two benzene rings (naphthalene) at these carbons. The S26—Cl29 bond distance is the longest (2.149 Å). The longest S26—Cl29 distance attributes the pure single bond character. The mean ring C—H bond length determined by B3LYP/6-311++G(d,p) method is 1.095 Å while the mean C—H bond distance in naphthalene ring is 1.082 Å. This suggests that the influence of the methyl groups substituent on the skeletal molecular parameters of dansyl chloride seems to be negligibly small.

Optimized geometry shows that dansyl chloride molecular structure is not planar as it is evident from C13—C9—S26—O28 and C6—C5—N17—C18 dihedral angles are 139.5° and −108.5° respectively. The calculated dihedral angles C1—C2—C3—C9 (178.7°), C2—C3—C4—C10 (174.1°) and C10—C4—C5—C6 (−172.5°) show that the naphthalene ring is coplanar. Since, large deviation from experimental C—H bond length may arise from the

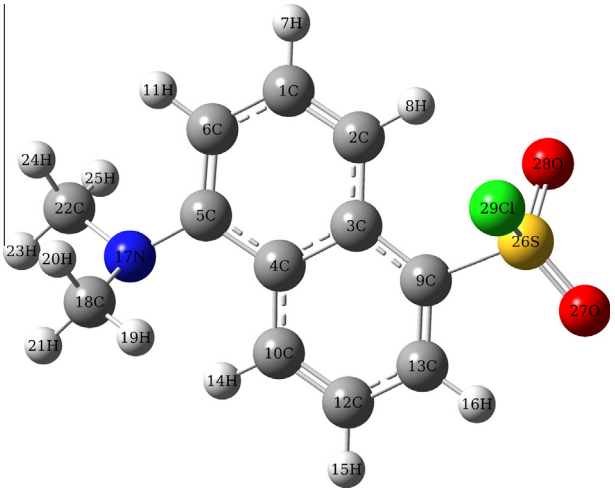

Fig. 1. Molecular structure with atom numbering scheme of dansyl chloride.

Table 1
Comparison of the geometrical parameters of dansyl chloride, bond lengths in angstrom, angles in degrees.

Bond lengths	[a]Exp	B3LYP	Bond angles	[a]Exp	B3LYP	Bond angles	[a]Exp	B3LYP
C1—C2	1.369	1.373	C2—C1—C6	121.4	121.6	O27—S26—O28	118.4	120.9
C1—C6	1.411	1.408	C1—C2—C3	120.1	119.8	C9—S26—O27	–	109.5
C2—C3	1.421	1.418	C2—C3—C4	118.9	119.1	C9—S26—O28	–	111.6
C3—C4	1.431	1.437	C2—C3—C9	124.0	124.7	C9—S26—Cl29	–	101.1
C3—C9	1.435	1.431	C4—C3—C9	117.1	116.2	C—C—$H_{average}$	119.7	119.7
C4—C5	1.438	1.440	C3—C4—C5	119.6	119.6	N—C—$H_{average}$	109.5	110.7
C4—C10	1.423	1.417	C3—C4—C10	119.2	119.4	H—C—$H_{average}$	109.5	108.2
C5—C6	1.377	1.382	C5—C4—C10	121.1	121.0	Dihedral angles		
C5—N17	1.418	1.418	C4—C5—C6	119.2	118.8	C1—C2—C3—C9	177.0	178.7
C9—C13	1.372	1.377	C4—C5—N17	117.8	118.5	C2—C3—C4—C10	177.0	174.1
C9—S26	1.775	1.797	C6—C5—N17	123.1	122.6	C10—C4—C5—C6	−174.4	−172.5
C10—C12	1.362	1.374	C1—C6—C5	120.7	120.9	C10—C4—C5—N17	3.2	6.1
C12—C13	1.408	1.406	C3—C9—C13	121.9	123.1	C1—C6—C5—N17	−179.0	178.7
N17—C18	1.469	1.468	C3—C9—S26	121.7	122.2	C4—C5—N17—C18	71.7	73.0
N17—C22	1.456	1.458	C13—C9—S26	116.5	114.7	C4—C5—N17—C22	−158.2	−153.4
S26—O27	1.433	1.452	C4—C10—C12	121.5	121.7	C6—C5—N17—C18	−110.8	−108.5
S26—O28	1.443	1.453	C10—C12—C13	120.2	120.0	C6—C5—N17—C22	19.3	25.1
S26—Cl29	–	2.149	C9—C13—C12	120.0	119.3	C3—C9—C13—C12	−0.6	1.9
C—$H_{ring,\ average}$	0.950	1.082	C5—N17—C18	114.5	115.1	S26—C9—C13—C12	−178.4	−177.5
C—$H_{methyl,\ average}$	0.980	1.095	C5—N17—C22	115.6	116.7	C3—C9—S26—O27	−178.9	−176.3
			C18—N17—C22	110.4	111.5	C3—C9—S26—O28	−49.8	−39.8
			O27—S26—Cl29	106.5	105.9	C13—C9—S26—O27	2.0	3.0
			O28—S26—Cl29	109.5	105.8	C13—C9—S26—O28	131.2	139.5

[a] Taken from Ref. [36].

low scattering factors of hydrogen atoms in the X-ray diffraction experiment. The experimental values of C—H bond lengths is ~0.95 Å, while the value in the theoretical results are bigger than 1 Å. The interaction of the SO_2Cl and $N(CH_3)_2$ groups on the naphthalene ring is of great importance in determining its structure and vibrational properties. It is observed that the influence of the substituent on the molecule play a vital role particularly in the C—C bond distance of the ring carbon atoms. As it is evident from the bond lengths of C3—C9, C9—C13 (ring 2) and C3—C4, C5—C6 (ring 1) is 1.431 Å, 1.377 Å and 1.437 Å, 1.382 Å respectively show slight deviation when compared with C10—C12 and C1—C2 of 1.374 Å (ring 1) and 1.373 Å (ring 2), and symmetry of naphthalene ring is distorted, yielding ring angles smaller and larger than the normal value of 120° exactly at the substitution as shown in Table 1. The C1—C2—C3 angle is 119.8° and C4—C10—C12 angle is 121.7° for ring 1 and 2.

The C9—S26 bond length calculated by B3LYP/6-311++G(d,p) method is 1.797 Å is longer than that of X-ray data of related molecule by 0.022 Å [36]. The S—Cl bond length in p-iodobenzene sulfonyl chloride was calculated by B3LYP method is 2.401 Å [37]. For our title molecule, the corresponding bond length is 2.149 Å by B3LYP/6-311++G(d,p) method. From the theoretical values, it can be found that most of the optimized bond lengths are slightly higher than the experimental values. The largest deviations of bond lengths and bond angles between the theoretical and experimental ones are 0.183 and 1.6 Å. The deviations can be attributed to the fact that the theoretical calculations were aimed at the isolated molecules in the gaseous phase and the experimental results were aimed at the molecule in the solid state. Despite these differences, the calculated geometrical parameters represent good approximation, and they are the basis for the calculations of other parameters such as vibrational frequencies and thermodynamic parameters.

Vibrational assignments

The vibrational spectrum is mainly determined by the modes of the free molecule observed at higher wavenumbers, together with the lattice (translational and vibrational) modes in the low wavenumber region. In our present study, we have performed a frequency calculation analysis to obtain the spectroscopic signature of DC. The DC molecule consists of 29 atoms therefore they have 81 normal modes of vibration. All the frequencies are assigned in terms of fundamental, overtone and combination bands. Assignments have been made on the basis of relative intensities, energies, line shape and total energy distribution (TED). The measured (FT-IR and FT-Raman) wavenumbers and assigned wavenumbers of the some selected intense vibrational modes calculated at the B3LYP level using basis set 6-311++G(d,p) along with their TED are given in Table 2. For B3LYP with 6-311++G(d,p) basis set, the wavenumbers in the ranges from 4000 to 1700 cm^{-1} and lower than 1700 cm^{-1} are scaled with 0.958 and 0.983 respectively [38]. The calculated Raman and IR intensities were used to convolute each predicted vibrational mode with a Lorentzian line shape with a full width at half maximum (FWHM = 10 cm^{-1}) to produce simulated spectra. This reveals good correspondence between theory and experiment in main spectral features. The experimental and theoretical FT-IR and FT-Raman spectra are shown in Fig. 2.

C—C vibrations

Naphthalene ring stretching vibrations are expected in the region 1620–1390 cm^{-1}. Naphthalene ring vibrations are found to make a major contribution in the IR and Raman spectra [39,40], the frequency observed in FT-IR spectrum at 1654, 1603, 1571 and 1521 cm^{-1} and in FT-Raman spectrum at 1630, 1602, 1574 and 1517 cm^{-1} are assigned to C—C stretching vibrations. The theoretically predicted harmonic frequencies at 1619, 1597, 1577 and 1510 cm^{-1} (mode Nos. 13–16) by B3LYP/6-311++G(d,p) show a good agreement with experimental data. These vibrations are mixed up with C—H in-plane bending vibrations as shown in Table 2. The TED corresponds to these vibrations are mixed modes as evident from Table 2.

C—H vibrations

The hetero aromatic structure shows the presence of C—H stretching vibration in the region 3100–3000 cm^{-1} which is the characteristic region for the ready identification of C—H stretching vibration [41,42]. In this region the bands are not affected appreciably by the nature of substituent. Two benzene rings are fused together in naphthalene ring of DC molecule; it has three

Table 2
Comparison of the experimental and calculated vibrational wavenumbers and proposed assignments of dansyl chloride.

	Experimental			B3LYP/6-311++g(d,p)				Assignments of vibrational modes
No.	FT-IR	FT-Raman	Unscaled	Scaled	I_{IR}	SA_{Ra}	I_{Ra}	Assignments and TED ($\geqslant$6%)
1	3392		3238	3102	3.600	62.772	0.005	υ CH (98)
2		3084	3214	3079	4.545	140.168	0.012	υ CH (100)
3			3209	3074	3.878	69.608	0.006	υ CH (100)
4	3059		3199	3065	8.843	129.774	0.012	υ CH (99)
5			3185	3052	3.927	104.589	0.010	υ CH (100)
6	3039	3032	3175	3042	9.884	98.182	0.009	υ CH (99)
7			3131	2999	14.956	32.315	0.003	υ_{asym} CH_2 of CH_3 (99)
8	2967	2966	3114	2983	16.676	67.412	0.007	υ_{asym} CH_2 of CH_3 (99)
9			3064	2935	52.878	238.573	0.025	υ_{sym} CH_2 of CH_3 (99)
10			3062	2934	14.383	54.558	0.006	υ_{sym} CH_2 of CH_3 (96)
11	2835		2957	2833	114.895	227.513	0.028	υ_{sym} CH_3 (98)
12			2945	2821	70.980	132.811	0.016	υ_{sym} CH_3 (95)
	2637							
	2455							
	2361							
	2343							
13	1654	1630	1647	1619	16.767	30.924	0.025	υ CC (71)
14	1603	1602	1625	1597	13.086	1.589	0.001	υ CC (77)
15	1571	1574	1604	1577	82.967	296.180	0.255	υ CC (68)
16	1521	1517	1536	1510	6.185	6.596	0.006	υ CC (71)
17	1493		1525	1499	18.412	29.794	0.029	ρ CH_2 of CH_3 (80)
18			1507	1481	9.428	1.167	0.001	ρ CH_2 of CH_3 (81)
19			1498	1473	9.288	4.935	0.005	ρ CH_2 of CH_3 (54) + β CH of CH_3 (17)
20	1469	1469	1491	1466	46.225	14.444	0.015	β CH_{ring} (32) + ρ CH_2 of CH_3 (16) + υ CC (11)
21	1458		1484	1459	9.355	9.201	0.010	ρ CH_2 of CH_3 (75) + β CH of CH_3 (10)
22			1471	1446	4.178	37.892	0.041	CH_3 umbrella (73)
23	1424	1430	1446	1422	2.195	15.037	0.017	CH_3 umbrella (96)
24			1439	1415	18.655	42.420	0.049	β CH_{ring} (37) + υ CC (25)
25	1396	1402	1427	1403	33.036	5.321	0.006	β CH_{ring} (48) + υ CC (20)
26	1381		1368	1345	49.903	366.525	0.485	Ring deformation (77)
27	1363	1357	1359	1336	7.549	23.661	0.032	Ring deformation (65)
28			1340	1318	58.768	20.625	0.029	υ CN (30) + r CH_3 (26)
29			1329	1307	129.765	9.852	0.014	υ_{asym} SO_2 (94)
30	1237	1244	1263	1242	24.061	7.162	0.012	υ CC (29) + β CH_{ring} (27)
31	1218	1213	1228	1207	7.791	4.677	0.008	υ CC (37) + β CH_{ring} (34)
32	1204		1220	1200	9.379	1.263	0.002	β CH_{ring} (45) + υ CC (28)
33			1210	1189	12.344	3.272	0.006	υ_{asym} N $(CH_3)_2$ (34) + r CH_3 (17) + β CH_{ring} (15)
34	1182	1182	1201	1181	10.444	3.919	0.007	β CH_{ring} (38) + υ CC (11) + r CH_3 (10)
35	1161	1159	1176	1156	2.293	6.379	0.013	β CH_{ring} (47) + υ CC (16)
36	1146		1168	1148	19.682	24.004	0.048	r CH_3 (87)
37			1127	1108	206.422	77.060	0.168	υ_{sym} SO_2 (64)
38	1096	1099	1118	1099	75.870	21.950	0.049	r CH_3 (32) + υ_{sym} SO_2 (24) + υ CC (16)
39			1112	1093	2.323	14.369	0.032	r CH_3 (33) + υ CC (29)
40	1074	1073	1091	1072	12.485	1.846	0.004	υ CC (62)
41	1037		1070	1052	22.099	3.486	0.009	r CH_3 (47) + υ_{asym} N $(CH_3)_2$ (25)
42	1023	1027	1057	1039	26.721	4.598	0.012	υ N—CH_3 (21) + υ CC (16) + β CCC (11) + r CH_3 (11)
43			1014	997	0.691	1.503	0.004	γ CH_{ring} (92)
44	983	987	995	978	0.917	1.920	0.006	γ CH_{ring} (86)
45			959	943	0.132	0.381	0.001	γ CH_{ring} (87)
46	936	938	951	935	33.069	3.721	0.012	υ_{sym} N $(CH_3)_2$ (48)
47	902	902	912	896	1.175	0.612	0.002	γ CH_{ring} (87)
48			849	834	3.376	20.170	0.088	Ring breathing (72)
49	825	835	834	820	1.058	1.226	0.006	γ CH_{ring} (32) + γ CCCC (30)
50		796	807	793	74.249	1.582	0.008	γ CH_{ring} (78)
51	787		802	789	13.224	2.826	0.014	Ring deformation (71)
52	773	775	773	760	7.650	6.280	0.034	Ring deformation (65)
53	723		752	739	3.083	0.933	0.005	γ CH_{ring} (58)
54	677	681	681	669	10.494	2.582	0.019	γ CCCC (46)
	666	664						
	642	641						
55	607	612	617	607	63.445	21.281	0.195	Ring breathing (39) + υ CN (12) + υ CS (8)
56	588	587	593	583	1.170	2.390	0.024	γ CCCC (76)
57	558	558	569	559	110.196	10.229	0.112	γ CCCS (24) + β SOCl (16) + β CSO (14)
58	530	531	543	534	25.197	5.256	0.064	β CCC (48)
59			535	526	35.612	2.894	0.036	β CCC (62)
60	510		532	523	62.784	2.899	0.037	β OSO (49)
61	494	494	500	491	15.569	6.188	0.091	β CCC (38) + β C—N—CH_3 (12)
62	485		476	468	34.658	3.819	0.062	γ CCCC (50)
63	431	433	473	465	58.829	25.767	0.426	γ CCCC (44)
64		381	391	384	2.588	11.526	0.289	ρ CH_3—N—CH_3 (59)
65			348	342	3.284	5.942	0.191	β C—N—CH_3 (14) + β CSO (9)
66			347	341	5.188	1.495	0.048	β C—N—CH_3 (37) + υ CS (9)

(*continued on next page*)

Table 2 (*continued*)

No.	Experimental			B3LYP/6-311++g(d,p)				Assignments of vibrational modes
	FT-IR	FT-Raman	Unscaled	Scaled	I_{IR}	SA_{Ra}	I_{Ra}	Assignments and TED (⩾6%)
67		328	326	320	13.327	26.944	1.000	υ S—Cl (64) + w SO_2 (12)
68			323	317	4.614	10.137	0.384	t SO_2 (28) + υ S—Cl (15)
69		297	284	279	2.649	2.646	0.002	τ CH_3 (56) + υ S—Cl (12)
70		269	274	270	0.622	9.118	0.006	τ CH_3 (52) + υ S—Cl (12)
71			269	264	0.394	0.111	0.000	t SO_2 (29) + γ CCCC (21)
72			253	249	1.130	3.213	0.002	t SO_2 (67)
73		209	228	224	0.581	3.779	0.003	τ CH_3 (68)
74			193	190	1.164	0.783	0.001	r SO_2 (42)
75		175	174	171	2.219	0.582	0.001	Butterfly (ring) (64)
76			160	157	1.416	3.046	0.004	r $N(CH_3)_2$ (22) + butterfly (ring) (19) + β C—S—Cl (11)
77		118	139	137	1.720	2.623	0.004	w $N(CH_3)_2$ (24) + r SO_2 (26) + β CCC (10)
78		97	106	105	0.321	4.763	0.009	r $N(CH_3)_2$ (29) + β C—S—Cl (20)
79		61	80	79	1.963	5.771	0.015	t $N(CH_3)_2$ (76)
80			43	42	0.014	3.638	0.018	τ SO_2Cl (86)
81			38	38	0.189	2.118	0.012	γ ring-SO_2Cl (45) + γ ring-$N(CH_3)_2$ (21)

I_{IR}, I_{Ra}-IR and Raman Intensity (K mmol^{-1}), SA_{Ra}-Raman scattering activity (A^4 amu^{-1}), ν_{sym}-symmetric stretching; ν_{asym}-asymmetric stretching; β-in-plane bending; γ-out-of-plane bending; ρ-scissoring; t-twisting; r-rocking; w-wagging; τ-torsion. The out-of-plane banded atoms were underlined.

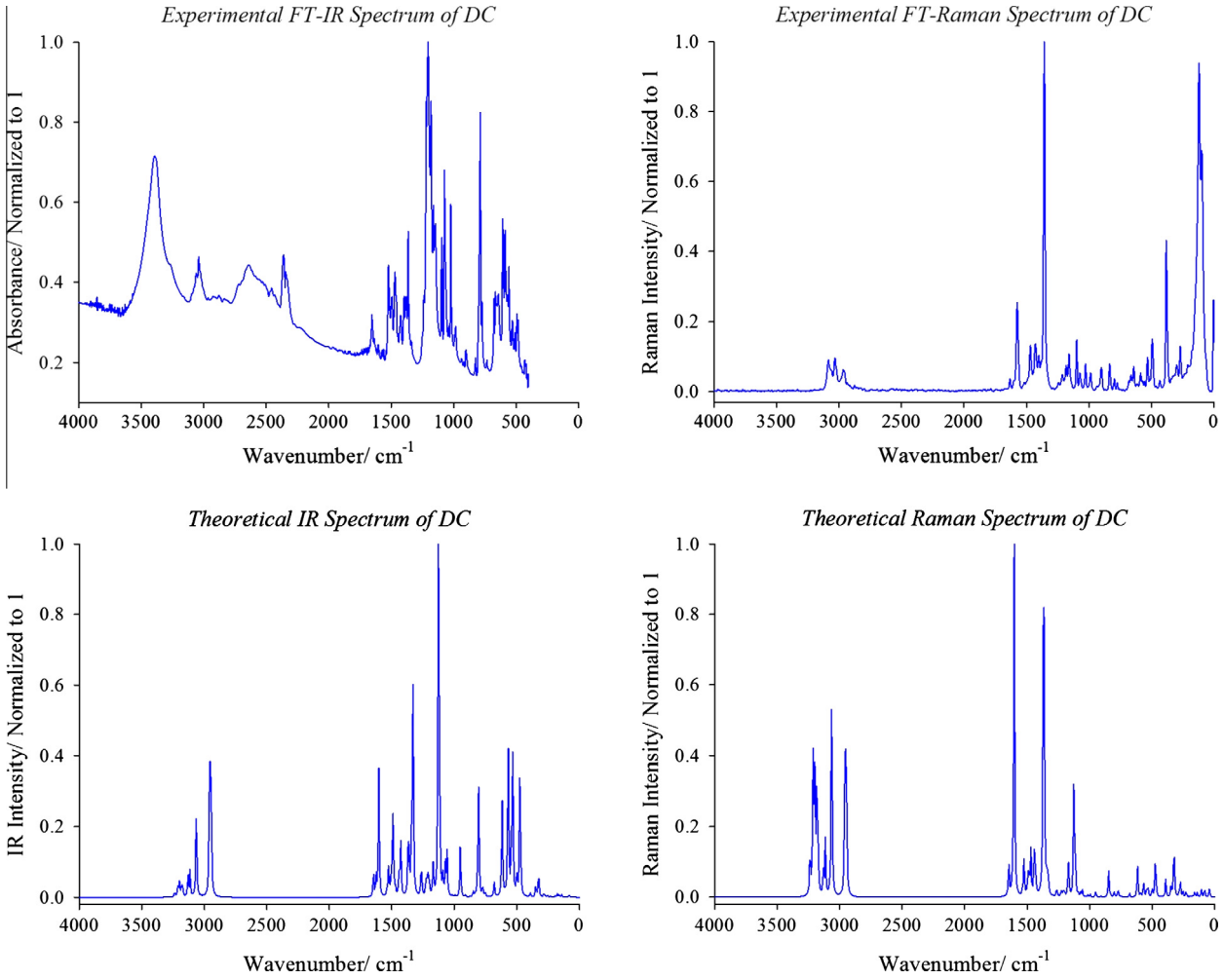

Fig. 2. Experimental and theoretical FT-IR and FT-Raman spectra of dansyl chloride.

adjacent C—H moieties in each benzene ring. The expected six C—H stretching vibrations are corresponding to stretching modes of C1—H, C2—H, C6—H, C10—H, C12—H and C13—H units. The weak bands in FT-IR spectrum at 3059, 3039 cm^{-1} and 3084, 3032 cm^{-1} in FT-Raman spectrum is assigned to C—H stretching vibration. The harmonic vibrations (mode Nos. 1–6) by B3LYP/6-311++G(d,p) method predicted at 3102, 3079, 3074, 3065, 3052 and 3042 cm^{-1} fall within the recorded spectral range. As expected, these modes are pure stretching modes as it is evident from TED column; they are exactly contributing to 100%.

The in-plane aromatic C—H bending vibration occurs in the region 1400–1000 cm^{-1}, the bands are sharp but weak and medium

intensity. The C—H in-plane bending vibrations computed at 1415, 1403, 1200, 1181 and 1156 cm^{-1}(mode Nos. 24, 25, 32 and 34–35) by B3LYP method show a good agreement with medium FT-IR band at 1396, 1204, 1182, 1161 cm^{-1} and 1402, 1182, 1159 cm^{-1} in FT-Raman spectrum. The TED corresponds to this mode is a mixed mode as it is evident in the Table 2.

The bands observed at 983, 902, 825 cm^{-1} in FT-IR and 987, 902, 835 and 796 cm^{-1} in FT-Raman spectrum are assigned to C—H out-of-plane bending vibrations of naphthalene ring of DC. This also shows good agreement with theoretical harmonic wavenumber values at 997, 978, 943, 896, 820 and 793 cm^{-1} (mode Nos. 43–45, 47 and 49–50) by B3LYP method. The TED also shows mixed contributions of approximately 80–90% for these vibrations.

SO_2 vibrations

The symmetric and asymmetric SO_2 stretching vibrations occur in the region 1125–1150 cm^{-1} and 1295–1330 cm^{-1} [43,44]. It is stated that in p-iodobenzene sulfonyl chloride [45], the SO_2 symmetric and asymmetric stretching vibrations occur at 1112 cm^{-1} and 1386 cm^{-1} respectively. For our title molecule, the antisymmetric (υ_{as}) stretching mode of SO_2 is calculated at the higher wavenumber 1307 cm^{-1} than the symmetric (υ_s) stretching mode of SO_2 at 1108 cm^{-1} by B3LYP/6-311++G(d,p) method having mode Nos. 29 and 37 as seen in Table 2. The experimental FT-IR and FT-Raman spectra do not show any such band in these regions. The SO_2 in-plane and out-of-plane bending vibrations for our title molecule are predicted at 317, 264, 249 and 190 cm^{-1} respectively.

N—$(CH_3)_2$ group vibrations

The CH_2 or CH_3 groups next to the nitrogen atom in amines are somewhat shifted. The symmetric stretch at 2770–2830 cm^{-1} is lowered in frequency and intensified and so stands out among other aliphatic bands [46,47]. For the compounds containing N—$(CH_3)_2$ group (in the aromatic structure) the stretching vibrations of N—$(CH_3)_2$ group occur in the region 2790–2810 cm^{-1} [48]. Ourselves have predicted the Raman band at 2809 cm^{-1} in 4-N-N′-dimethylamino pyridine [49]. In the case of DC which contains two benzene ring fused together will give N—$(CH_3)_2$ asymmetric and symmetric stretching vibration predicted at 1189 cm^{-1} (mode No. 33) and 935 cm^{-1} respectively (mode No. 46) by B3LYP method. The TED of these vibration shows that they are mixed mode contributing 34% for asymmetric and 48% for symmetric N—$(CH_3)_2$ stretching vibration.

Methyl group vibrations

Vibrational spectral studies on methyl pyridine have shown that asymmetric and symmetric methyl stretching band can be observed around 2846 and 2960 cm^{-1}, respectively [50–53]. For the assignments of CH_3 group one can expect that nine fundamentals can be associated to each CH_3 group, namely the symmetrical stretching in CH_3 (CH_3 symmetric stretch) and asymmetrical stretching (CH_3 asymmetric stretch), in-plane stretching modes (i.e. in-plane hydrogen stretching mode), the symmetrical (CH_3 symmetric deform) and asymmetrical (CH_3 asymmetric deform) deformation modes, the in-plane rocking (CH_3 ipr), out-of-plane rocking (CH_3 opr) and twisting (tCH_3) bending modes. For the methyl group compound [54], the asymmetric stretching mode appears in the range 2825–2870 cm^{-1}, lower in magnitude compared to its value in CH_3 (compounds) (2860–2935 cm^{-1}) whereas the asymmetric stretching modes for both the type of compounds lie in the same region 2925–2985 cm^{-1}. The medium bands observed at 2967 cm^{-1} in the FT-IR spectrum could be attributed to CH_3 asymmetric stretching vibration. The same vibration appears in the FT-Raman spectrum at 2966 cm^{-1} with medium weak intensity. The theoretically two computed values at 2999 and 2983 cm^{-1} show excellent agreement with experimental observations. The bands observed at 2835 cm^{-1} in FT-IR spectrum could be attributed to CH_3 symmetric stretching vibration. The theoretically computed value for symmetric stretching vibration at 2935, 2934, 2833 and 2821 cm^{-1} also shows excellent agreement with experimental observation.

The asymmetric and symmetric bendings are recorded in the 1410–1455 cm^{-1} region and about 1375 cm^{-1}, respectively, while the rocking mode appear in the 990–1050 cm^{-1}. Predicted by the DFT calculation, the series of bands appearing in the 1400–1500 cm^{-1} region are mainly due to the methyl deformation coupling with the ring C—C—H bending and C—C stretching motions, to different extents and in different ways. In the case of DC a band observed at 1424 cm^{-1} in FT-IR and at 1430 cm^{-1} in FT-Raman spectrum correspond to CH_3 deformation and correlated with the calculated frequency at 1446 and 1422 cm^{-1}. This behavior can be found in other fundamentals such as symmetric deformation and rocking modes. The torsion vibrations are not observed in the FT-IR spectrum because these appear at very low frequency. The scaling procedure predicts that these vibrations could appear at about 279, 270 and 224 cm^{-1} in dansyl chloride. The FT-Raman experimental observations at 297, 269 and 209 cm^{-1} show an excellent agreement with theoretical results. These assignments find support from the work of Singh and Prasad [55] and are within the frequency intervals given by Varsanyi [56].

Nonlinear optical effects

Nonlinear optical (NLO) effects arise from the interactions of electromagnetic fields in various media to produce new fields altered in phase, frequency, amplitude or other propagation characteristics from the incident fields [57]. NLO is at the forefront of current research because of its importance in providing the key functions of frequency shifting, optical modulation, optical switching, optical logic, and optical memory for the emerging technologies in areas such as telecommunications, signal processing, and optical interconnections [58–61].

The first hyperpolarizability (β_0) of this novel molecular system, and related properties (β, α_0 and $\Delta\alpha$) of dansyl chloride are calculated using B3LYP/6-311++G(d,p) method, based on the finite-field approach. In the presence of an applied electric field, the energy of a system is a function of the electric field. First order hyperpolarizability is a third rank tensor that can be described by $3 \times 3 \times 3$ matrices. The 27 components of the 3D matrix can be reduced to 10 components due to the Kleinman symmetry [62]. It can be given in the lower tetrahedral format. It is obvious that the lower part of the $3 \times 3 \times 3$ matrices is a tetrahedral. The components of β are defined as the coefficients in the Taylor series expansion of the energy in the external electric field. When the external electric field is weak and homogeneous, this expansion becomes:

$$E = E^0 - \mu_\alpha F_\alpha - 1/2\alpha_{\alpha\beta}F_\alpha F_\beta - 1/6\beta_{\alpha\beta\gamma}F_\alpha F_\beta F_\gamma + \ldots\ldots$$

where E^0 is the energy of the unperturbed molecules, F_α is the field at the origin, μ_α, $\alpha_{\alpha\beta}$ and $\beta_{\alpha\beta\gamma}$ are the components of dipole moment, polarizability and the first order hyperpolarizabilities, respectively. The total static dipole moment μ, the mean polarizability α_0, the anisotropy of the polarizability $\Delta\alpha$ and the mean first order hyperpolarizability β_0, using the x, y, z components they are defined as:

$$\mu = \left(\mu_x^2 + \mu_y^2 + \mu_z^2\right)^{1/2}$$

$$\alpha_0 = (\alpha_{xx} + \alpha_{yy} + \alpha_{zz})/3$$

$$\alpha = 2^{-1/2}\left[(\alpha_{xx} - \alpha_{yy})^2 + (\alpha_{yy} - \alpha_{zz})^2 + (\alpha_{zz} - \alpha_{xx})^2 + 6\alpha_{xx}^2\right]^{1/2}$$

$$\beta_0 = \left(\beta_x^2 + \beta_y^2 + \beta_z^2\right)^{1/2}$$

and

Table 3
The electric dipole moment, polarizability and first order hyperpolarizability of dansyl chloride.

	a.u.	esu ($\times 10^{-24}$)		a.u.	esu ($\times 10^{-30}$)
α_{xx}	214.0665962	31.725	β_{xxx}	−701.06	−6.057
α_{xy}	−6.7028252	−0.993	β_{xxy}	−102.66	−0.887
α_{yy}	206.9824909	30.675	β_{xyy}	40.62	0.351
α_{xz}	57.6763228	8.548	β_{yyy}	59.69	0.516
α_{yz}	−6.1336836	−0.909	β_{xxz}	−439.65	−3.798
α_{zz}	174.9045177	25.921	β_{xyz}	−72.10	−0.623
α_{tot}	198.6512016	29.440	β_{yyz}	76.69	0.663
$\Delta\alpha$	107.3952937	15.916	β_{xzz}	−290.41	−2.509
			β_{yzz}	−115.49	−0.998
			β_{zzz}	76.67	0.662
			β_{tot}	1005.58	8.687

$$\beta_x = \beta_{xxx} + \beta_{xyy} + \beta_{xzz}$$
$$\beta_y = \beta_{yyy} + \beta_{xxy} + \beta_{yzz}$$
$$\beta_z = \beta_{zzz} + \beta_{xxz} + \beta_{yyz}$$

Since the values of the polarizabilities (α) and hyperpolarizability (β) of the Gaussian 03 output are reported in atomic units (a.u.), the calculated values have been converted into electrostatic units (esu) (α: 1 a.u. = 0.1482×10^{-24} esu; β: 1 a.u. = 8.639×10^{-33} esu).

Urea is one of the prototypical molecules used in the study of the NLO properties of molecular systems. Therefore it was used frequently as a threshold value for comparative purposes. The total molecular dipole moment and the first order hyperpolarizability are 7.19 Debye and 8.687×10^{-30} esu, respectively and are depicted in Table 3. Total dipole moment of title molecule is approximately five times greater than that of urea and the first order hyperpolarizability of title molecule is 23 times greater than that of urea (μ and β of urea are 1.3732 Debye and 0.3728×10^{-30} esu obtained by HF/6-311G(d,p) method). These results indicate that the title compound is a good candidate of NLO material.

To understand this phenomenon in the context of molecular orbital theory, we examined the molecular HOMOs and molecular LUMOs of the title compound. When we see the first hyperpolarizability value, there is an inverse relationship between the first hyperpolarizability and HOMO–LUMO gap, allowing the molecular orbitals to overlap to have a proper electronic communication conjugation, which is a marker of the intramolecular charge transfer from the electron donating group through the π-conjugation system to the electron accepting group [63,64].

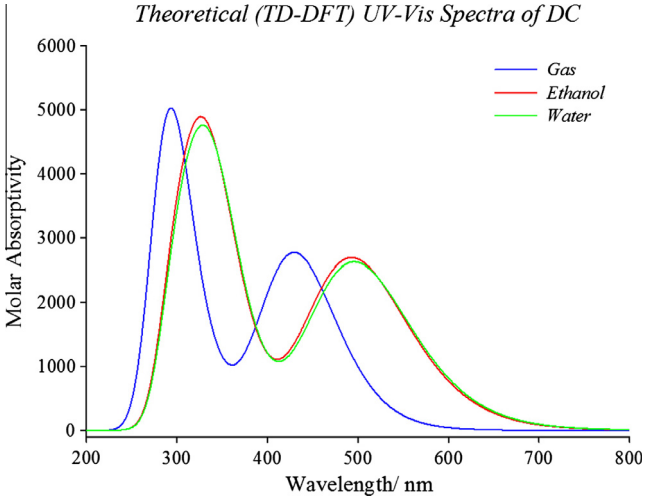

Fig. 4. Theoretical UV–Vis spectra of dansyl chloride.

Table 4
Theoretical and experimental electronic absorption spectra values of dansyl chloride.

Experimental			TD-DFT/6-311++G(d,p)		
Ethanol			Ethanol		
λ (nm)	Abs.	E (eV)	λ (nm)	E (eV)	f
			493.37 (70 → 71)	2.5130	0.0663
			364.16 (70 → 72)	3.4047	0.0249
			334.82 (69 → 71)	3.7030	0.0749
328.0	0.081	3.7805	324.60 (68 → 71)	3.8196	0.0077
246.5	0.288	5.0304	301.47 (70 → 73)	4.1127	0.0609
216.0	0.902	5.7407	272.67 (69 → 72)	4.5470	0.0014
Water			Water		
			496.18 (70 → 71)	2.4988	0.0647
			365.04 (70 → 72)	3.3965	0.0245
			336.11 (69 → 71)	3.6888	0.0742
312.0	0.107	3.9744	325.51 (68 → 71)	3.8090	0.0078
241.0	0.347	5.1452	301.84 (70 → 73)	4.1076	0.0578
215.5	0.926	5.7541	273.01 (69 → 72)	4.5414	0.0013
			Gas		
			429.95 (70 → 71)	2.8837	0.0681
			338.36 (70 → 72)	3.6643	0.0139
			308.70 (68 → 71)	4.0163	0.0013
			304.01 (69 → 71)	4.0782	0.0587
			285.42 (70 → 73)	4.3439	0.0747
			263.67 (69 → 72)	4.7023	0.0063

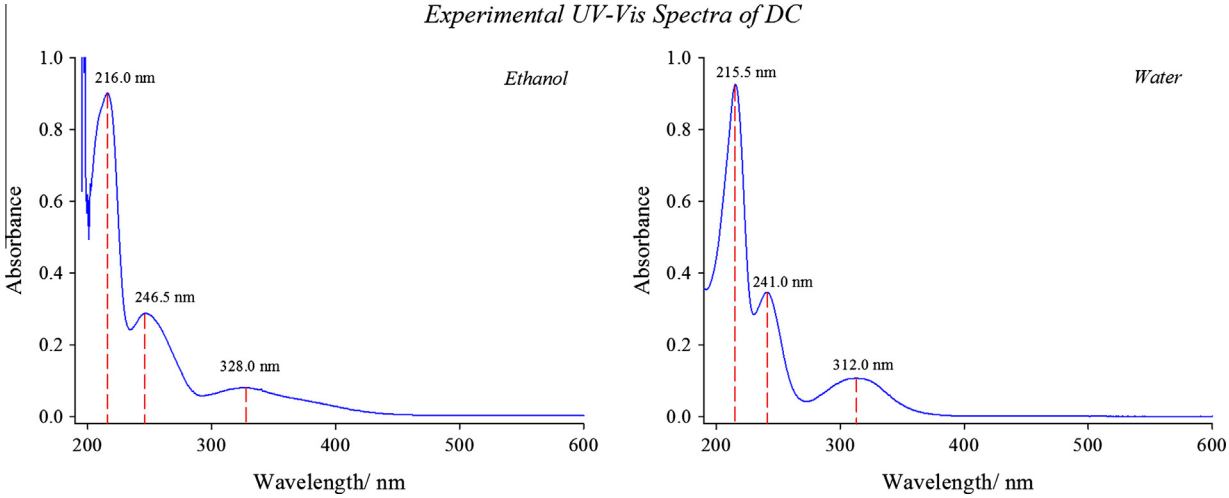

Fig. 3. Experimental UV–Vis spectra of dansyl chloride.

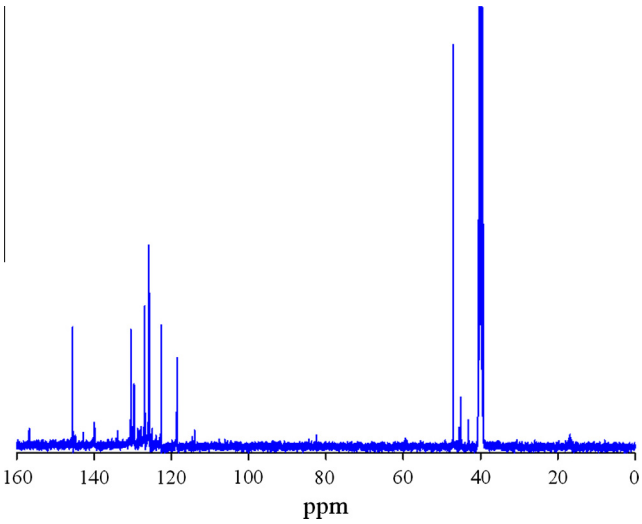

Fig. 5. Experimental ^{13}C NMR spectrum of dansyl chloride.

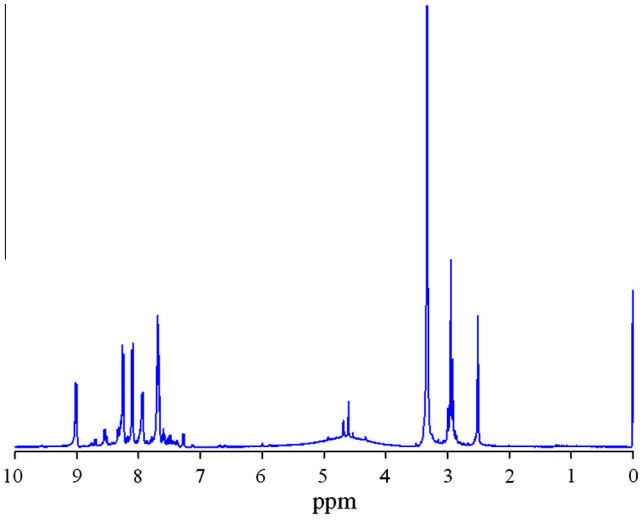

Fig. 6. Experimental ^{1}H NMR spectrum of dansyl chloride.

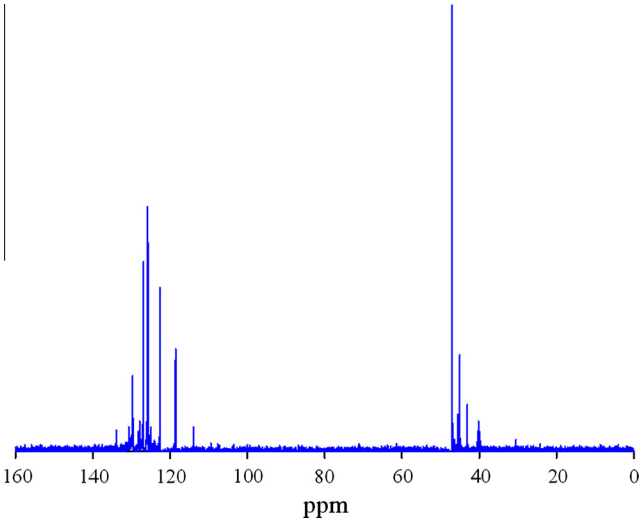

Fig. 7. DEPT 135 NMR spectrum of dansyl chloride.

Table 5
The observed (in DMSO) and predicted ^{1}H and ^{13}C NMR isotropic chemical shifts (with respect to TMS, all values in ppm) for dansyl chloride.

Atom	Exp (DMSO)	Gas	DMSO	Atom	Exp (DMSO)	Gas	DMSO
H7	7.69	7.59	7.86	C1	126.9	130.7	132.6
H8	9.01	8.70	8.93	C2	118.5	120.2	118.7
H11	7.94	7.06	7.40	C3	130.5	130.6	130.4
H14	8.25	8.60	8.54	C4	130.5	132.3	133.2
H15	7.69	7.32	7.64	C5	145.5	154.9	157.6
H16	8.10	8.07	8.23	C6	114.0	116.7	118.0
H19	2.93	2.87	2.99	C9	145.5	150.4	151.1
H20	2.93	2.15	2.32	C10	129.6	133.7	136.9
H21	2.93	2.75	2.96	C12	122.6	121.9	123.3
H23	2.93	2.64	2.83	C13	125.8	128.1	129.8
H24	2.93	2.74	2.95	C18	47.1	44.0	44.7
H25	2.93	2.57	2.66	C22	47.1	38.9	39.2

Table 6
Thermodynamic properties of dansyl chloride at different temperatures at the B3LYP/6-311++G(d,p) level.

T (K)	C (cal mol^{-1} K^{-1})	S (cal mol^{-1} K^{-1})	ΔH (kcal mol^{-1})
100	24.014	81.034	1.605
150	33.797	93.457	3.153
200	42.852	105.003	5.171
250	51.605	115.952	7.632
300	60.191	126.485	10.527
350	68.479	136.698	13.845
400	76.281	146.623	17.566
450	83.467	156.262	21.662
500	89.994	165.609	26.100
550	95.879	174.657	30.849
600	101.170	183.404	35.877
650	105.933	191.852	41.156
700	110.230	200.010	46.661

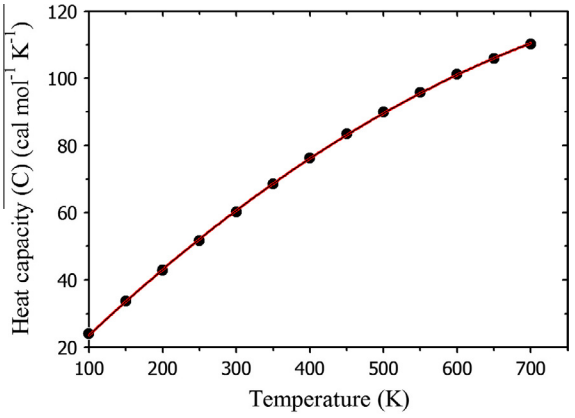

Fig. 8. Correlation graphic of heat capacity and temperature for dansyl chloride.

UV–Vis spectral analysis

The electronic absorption spectra of the title compound in ethanol and water as solvent were recorded within the 200–400 nm range and representative spectra are shown in Fig. 3. The theoretical UV–Vis spectra are shown in Fig. 4. As can be seen from the Fig. 3, electronic absorption spectra showed three bands at 328.0, 246.5 and 216.0 nm for ethanol, at 312.0, 241.0 and 215.5 nm for water. Electronic absorption spectra were calculated using the TD-DFT method based on the B3LYP/6-311++G(d,p) level optimized structure in gas phase. The calculated results are listed in Table 4 along with the experimental absorption spectral data. For TD-DFT calculations, the theoretical absorption bands are predicted at 429.95,

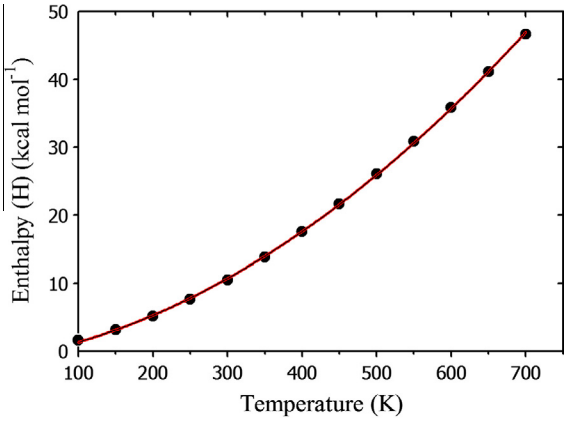

Fig. 9. Correlation graphic of enthalpy and temperature for dansyl chloride.

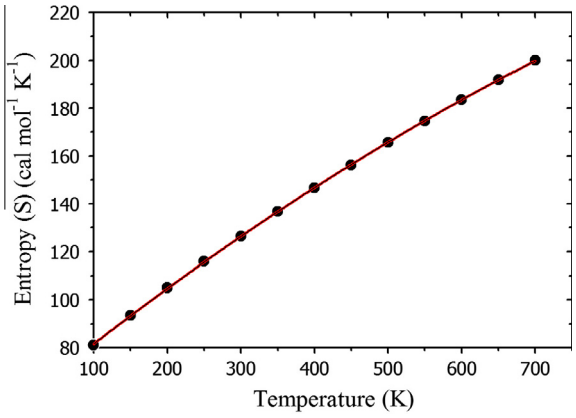

Fig. 10. Correlation graphic of entropy and temperature for dansyl chloride.

Table 7
Calculated energy values of dansyl chloride in its ground state.

Energy level	Gas	Ethanol	Water
E_{LUMO+2}	−1.3040	−1.1951	−1.1932
E_{LUMO+1}	−1.9228	−1.9652	−1.9685
E_{LUMO}	−2.7563	−2.9495	−2.9609
E_{HOMO}	−6.2102	−6.0184	−6.0135
E_{HOMO-1}	−7.3714	−7.2168	−7.2133
E_{HOMO-2}	−7.5621	−7.4609	−7.4595
$\Delta E_{(HOMO)-(LUMO)}$	−3.4540	−3.0689	−3.0526
$\Delta E_{(HOMO)-(LUMO+1)}$	−4.2875	−4.0532	−4.0450
$\Delta E_{(HOMO-1)-(LUMO)}$	−4.6151	−4.2673	−4.2524
$\Delta E_{(HOMO-2)-(LUMO)}$	−4.8058	−4.5114	−4.4986
$\Delta E_{(HOMO)-(LUMO+2)}$	−4.9063	−4.8233	−4.8203
$\Delta E_{(HOMO-1)-(LUMO+1)}$	−5.4486	−5.2516	−5.2448
Chemical hardness (η)	1.7270	1.5345	1.5263
Electronegativity (χ)	4.4833	4.4840	4.4872
Chemical potential (V)	−4.4833	−4.4840	−4.4872
Electrophilicity index (ω)	5.8194	6.5515	6.5960
Dipole moment (D)			
μ_x	7.0514	8.8760	8.9552
μ_y	1.1188	1.6135	1.6424
μ_z	0.8648	1.1776	1.1996
μ_{total}	7.1918	9.0980	9.1833

338.36, 308.70, 304.01, 285.42 and 263.67 nm in gas phase. In addition to the calculations in gas phase, TD-DFT calculations of the title compound in ethanol and water as solvent were performed using the PCM model. The PCM calculations reveal that the calculated absorption bands have slight red-shifts with the values of 493.37,

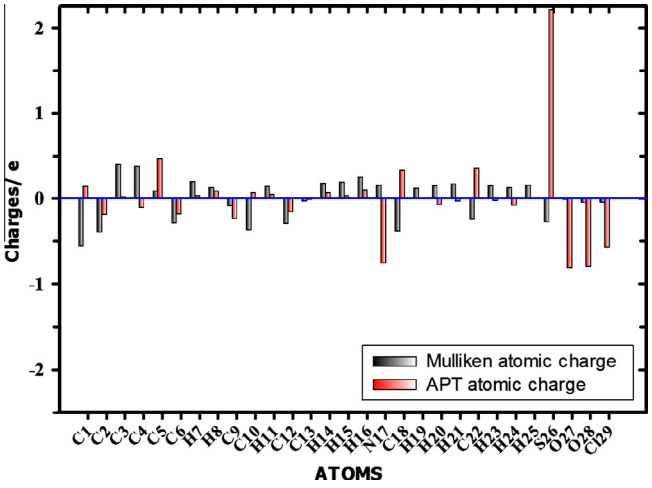

Fig. 11. Histogram of Mulliken and APT atomic charges for dansyl chloride.

Table 8
Mulliken and APT atomic charges of dansyl chloride.

Atom	Mulliken	APT
C1	−0.554	0.144
C2	−0.394	−0.185
C3	0.401	0.021
C4	0.374	−0.104
C5	0.087	0.465
C6	−0.283	−0.180
H7	0.198	0.035
H8	0.128	0.087
C9	−0.083	−0.237
C10	−0.366	0.069
H11	0.142	0.047
C12	−0.286	−0.154
C13	−0.030	−0.005
H14	0.178	0.069
H15	0.194	0.035
H16	0.253	0.103
N17	0.155	−0.752
C18	−0.382	0.334
H19	0.120	0.011
H20	0.148	−0.070
H21	0.173	−0.030
C22	−0.242	0.354
H23	0.150	−0.024
H24	0.128	−0.075
H25	0.159	0.004
S26	−0.272	2.216
O27	−0.010	−0.809
O28	−0.045	−0.796
Cl29	−0.041	−0.571

364.16, 334.82, 324.60, 301.47 and 272.67 nm in ethanol and 496.18, 365.04, 336.11, 325.51, 301.84 and 273.01 nm in water comparing with the gas phase calculations of TD-DFT method. Thus, the TD-DFT method in the gas phase and in solvent media is convenient for predicting electronic absorption spectra.

^{13}C and ^{1}H NMR spectral Analysis

The measured ^{13}C, ^{1}H and DEPT NMR spectra are shown in Figs. 5–7. The computed and experimental ^{13}C NMR and ^{1}H NMR chemical shifts are tabulated in Table 5. Aromatic carbons give signals in overlapped areas of the spectrum with chemical shift values from 100 to 150 ppm [65,66]. In our present investigation, the experimental chemical shift values of aromatic carbons are in the range 118.5–145.5 ppm. As can be seen from Table 5, the calculated values show good agreement with measured values of

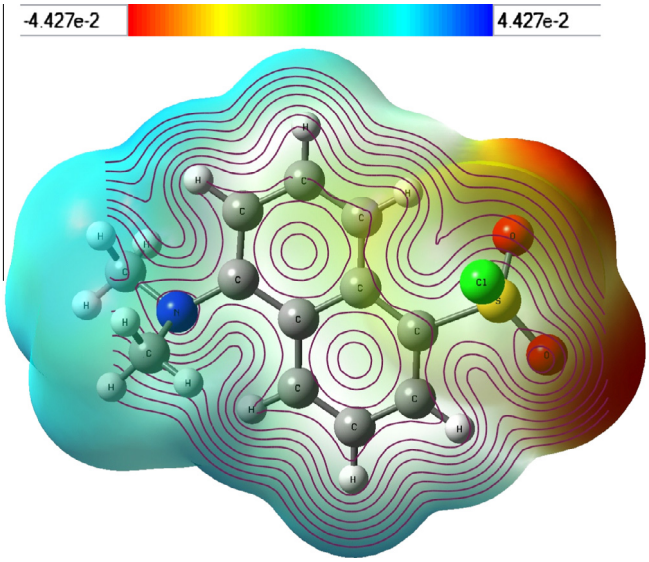

Fig. 12. Molecular electrostatic potential map of dansyl chloride.

^{1}H NMR chemical shifts. In addition, the present study, the two signals both at 47.1 ppm in ^{13}CNMR spectrum is assigned to C18 and C22 atom of methyl group.

Thermodynamic properties

On the basis of vibrational analysis, the statistically thermodynamic functions: heat capacity (C), enthalpy changes (H) and entropy (S) for the title molecule were obtained from the theoretical harmonic frequencies and are listed in Table 6. From the Table 6, it can be observed that these thermodynamic functions are increasing with temperature ranging from 100 to 700 K due to the fact that the molecular vibrational intensities increase with temperature. The correlation equations between heat capacity, enthalpy, entropy changes and temperatures were fitted by quadratic formulas and the corresponding fitting factors (R^2) for these thermodynamic properties are 0.9999, 0.9999 and 1.0000, respectively. The corresponding fitting equations are as follows and the correlation graphics of those shown in Figs. 8–10.

$$C = 2.0549 + 0.2255T - 0.0001 \times 10^{-5}T^2 \quad (R^2 = 0.9999)$$
$$H = -1.1497 + 0.0177T + 7.2958 \times 10^{-5}T^2 \quad (R^2 = 0.9999)$$
$$S = 57.1423 + 0.2509T - 6.7334 \times 10^{-5}T^2 \quad (R^2 = 1.0000)$$

All the thermodynamic data supply helpful information for the further study on the dansyl chloride. They can be used to compute the other thermodynamic energies according to relationships of thermodynamic functions and estimate directions of chemical reactions according to the second law of thermodynamics in thermochemical field. Notice: all thermodynamic calculations were done in gas phase and they could not be used in solution.

Ionization potential

By using HOMO and LUMO energy values for a molecule, the ionization potential and chemical hardness of the molecule were calculated using Koopman's theorem [67] and are given by $\eta = (I_P - E_A)/2$ where $I_P \approx -E(\text{HOMO})$, $E_A \approx -E(\text{LUMO})$, I_P = Ionization potential (eV), E_A = electron affinity (eV),

$$\eta = \left[\frac{E(\text{LUMO}) - E(\text{HOMO})}{2}\right]$$

The ionization potential of the DC in gas phase is 3.4539 eV. The ionization potential calculated for same molecule in ethanol as medium is 3.1689 eV. The calculated results are presented in Table 7. Considering the chemical hardness, large HOMO–LUMO gap means a hard molecule and small HOMO–LUMO gap means a soft molecule. One can also relate the stability of molecule to hardness, which means that the molecule with least HOMO–LUMO gap means it is more reactive.

Mulliken charge analysis

It is clear that Mulliken populations yield one of the simplest pictures of charge distribution and Mulliken charges render net atomic populations in the molecule. The charge distributions of DC have been calculated by B3LYP/6-311++G(d,p) level of theory and shown in Fig. 11. The results are shown in Table 8. As can be seen from the Table 8, the magnitudes of the carbon atomic charges, found to be either positive or negative, were noted to change from −0.55 to 0.40. All the hydrogen atoms, chlorine atom have a positive charge and nitrogen atom have a negative charge.

Molecular electrostatic potential

The different values of the electrostatic potential at the surface are represented by different colors. Potential increases in the order red < orange < yellow < green < blue. The color code of these maps is in the range between −27.778 kcal/mol (deepest red) and 27.778 kcal/mol (deepest blue) in the compound, where blue indicates the strongest attraction and red indicates the strongest repulsion. As can be seen from the MEP map of the title molecule, while regions having the negative potential are over the electronegative atom (nitrogen and chlorine atoms), the regions having the positive potential are over the hydrogen atoms. Fig. 12 provides a visual representation of the chemically active sites and comparative reactivity of the atoms.

Conclusions

The title molecular structure was characterized by FT-IR, FT-Raman, UV–Vis, ^{1}H and ^{13}C NMR spectroscopy. The molecular structural parameters, thermodynamic properties, vibrational frequencies and chemical shifts (^{1}H and ^{13}C) of the fundamental modes of dansyl chloride optimized geometry have been determined from ab initio DFT calculations. The geometry was optimized without any symmetry constrains using DFT/B3LYP method with 6-311++G(d,p) basis set. DFT calculations at B3LYP/6-311++G(d,p) level for the title molecule showed that the optimized geometry closely resembled the crystal structure. A comparison between calculated vibrational spectra and their experimental counterpart showed a good correlation. To fit the theoretical vibrational frequency results with experimental ones for B3LYP, we have multiplied by the scale factors 0.958 and 0.983 for the wavenumbers in the ranges from 4000 to 1700 cm^{-1} and lower than 1700 cm^{-1} respectively. The electric dipole moments and the first hyperpolarizabilities of the compound studied have been calculated by 6-311++G(d,p) method. Absorption maxima (λ_{max}) of dansyl chloride was calculated by TD-DFT method and compared with experimental UV–Vis spectra.

References

[1] Y. Ran, G.E. Fanucci, Anal. Biochem. 382 (2008) 132–134.
[2] M.S. Aqueel, V. Pathak, A.K. Pathak, Tetrahed. Lett. 49 (2008) 7157–7160.
[3] S. Fu, J. Biotechnol. 136 (2008) 193–200.
[4] H. Li, J. Kang, L. Ding, F. Lu, Y. Fang, J. Photochem. Photobiol. A 197 (2008) 226–231.

[5] W.-S. Li, M.-J. Teng, X.-R. Jia, B.-B. Wang, J.-M. Yeh, Y. Wei, Tetrahed. Lett. 49 (2008) 1988–1992.
[6] G. Weber, Biochem. J. 51 (1952) 155–167.
[7] W.R. Gray, B.S. Hartley, Biochem. J. 89 (1963) 59P.
[8] M. Ayad, M.H. Abdel-Hay, Analyst 109 (1984) 1431–1434.
[9] W. Baeyens, B. Lin, V. Corbisier, Analyst 115 (1990) 359–363.
[10] C. Cruces Blanco, F. Garcí a Sa´nchez, Analyst 116 (1991) 851–856.
[11] A.J. Tong, Y.G. Wu, L.D. Li, Talanta 43 (1996) 1429–1436.
[12] P. Clausing, L.G. Rushing, G.D. NewPort, J.F. Bowyer, J. Chromatogr. B. 692 (1997) 419–426.
[13] R.M. Linares, J.H. Ayala, A.M. Afonso, V. Gonzalez, Analyst 123 (1998) 725–729.
[14] J.M. Quirke, C.L. Adams, G.J. Van Berkel, Anal. Chem. 66 (1994) 1302–1315.
[15] W.Z. Shou, X. Jiang, W. Naidong, Biomed. Chromatogr. 18 (2004) 414–421.
[16] R. Miao, Q.-Y. Zheng, C.-F. Chen, Z.-T. Huang, Tetrahed. Lett. 45 (2004) 4959–4962.
[17] T. Kikuchi, M. Narita, F. Hamada, Tetrahedron 57 (2001) 9317–9324.
[18] Y. Zhang, Z.J. Guo, X.Z. You, J. Am. Chem. Soc. 123 (2001) 9378–9387.
[19] H. Tanak, A. Ağar, M. Yavuz, J. Mol. Mod. 16 (2010) 577–587.
[20] M.J. Frisch, et al., Gaussian 03, Revision B.01, Gaussian Inc., Pittsburgh, PA, 2003.
[21] R. Dennington, II, T. Keith, J. Millam, GaussView, Version 4.1.2, Semichem, Inc., Shawnee Mission, KS, 2007.
[22] M.H. Jamroz, Vibrational Enegy Distribution Analysis, VEDA 4 Computer Program, Poland, 2004.
[23] N.C. Handy, P.E. Maslen, R.D. Amos, J. Phys. Chem. 97 (1993) 4392–4396.
[24] M.A. Palafox, M. Gill, N.J. Nunez, V.K. Rastogi, L. Mittal, R. Sharma, Int. J. Quant. Chem. 103 (2005) 394–421.
[25] F.J. Devlin, J.W. Finley, P.J. Stephens, M.J. Frisch, J. Phys. Chem. 99 (1995) 16883–16902.
[26] A. Usha Rani, N. Sundaraganesan, M. Kurt, M. Cinar, M. Karabacak, Spectrochim. Acta A 75 (2010) 1523–1529.
[27] E. Runge, E.K.U. Gross, Phys. Rev. Lett. 52 (1984) 997–1000.
[28] R.E. Stratmann, G.E. Scuseria, M.J. Frisch, J. Chem. Phys. 109 (1998) 8218–8224.
[29] R. Bauernschmitt, R. Ahlrichs, Chem. Phys. Lett. 256 (1996) 454–464.
[30] M.E. Casida, C. Jamorski, K.C. Casida, D.R. Salahub, J. Chem. Phys. 108 (1998). 4439-449.
[31] S. Miertus, E. Scrocco, J. Tomasi, Chem. Phys. 55 (1981) 117–129.
[32] V. Barone, M. Cossi, J. Phys. Chem. A 102 (1998) 1995–2001.
[33] M. Cossi, N. Rega, G. Scalmani, V. Barone, J. Comput. Chem. 24 (2003) 669–681.
[34] J. Tomasi, B. Mennucci, R. Cammi, Chem. Rev. 105 (2005) 2999–3093.
[35] R. Dennington, II, T. Keith, J. Millam, Gauss View, Version 4.1.2, Semichem, Inc., Shawnee Mission, KS, 2007.
[36] P. Bhatt, T. Govender, H.G. Kruger, G.E.M. Maguire, Acta Cryst. E67 (2011) o2458–o2459.
[37] M. Arivazhagan, S. Prabhakaran, R. Gayathri, Spectrochim. Acta 82A (2011) 332–339.
[38] N. Sundaraganesan, S. Illakiamani, H. Saleem, P.M. Wojciechowski, D. Michalska, Spectrochim. Acta 61A (2005) 2995–3001.
[39] C. Surisseau, P. Marvel, J. Raman Spectrosc. 25 (1994) 447–451.
[40] A.J. Barnes, M.A. Majid, M.A. Stuckey, P. Gregory, C.V. Stead, Spectrochim. Acta 41A (1985) 629–635.
[41] V.K. Rastogi, M.A. Palafox, R.P. Tanwar, L. Mittal, Spectrometric Identification of Organic Compounds, Wiley, New York, 1981.
[42] N.B. Colthup, L.H. Daly, S.E. Wiberly, Introduction to Infrared and Raman Spectroscopy, third ed., Academic Press, Boston, MA, 1990.
[43] G. Socrates, Infrared Characteristics Group Frequencies, John Wiley and Sons, New York, 1980.
[44] N.P.G. Roeges, A Guide to the complete Interpretation of Infrared Spectra of Organic Structures, Wiley, New York, 1994.
[45] M. Arivazhagan, S. Prabharan, R. Gayathri, Spectrochim. Acta 82A (2011) 332–339.
[46] R.D. Hill, G.D. Meakins, J. Chem. Soc. (1958) 760–764.
[47] W.B. Wright Jr., J. Org. Chem. Soc. (1959) 1362–1370.
[48] N.B. Colthup, Introduction to Infrared and Raman Spectroscopy, Academic Press, New York, 1990.
[49] N. Sundaraganesan, S. Kalaichelvan, C. Meganathan, B.D. Joshua, J.P. Cornard, Spectrochim. Acta 71A (2008) 898–906.
[50] G. Socrates, Infrared Characteristic Group Frequencies, Wiley, New York, 1980.
[51] G. Varsanyi, Vibrational Spectra of Benzene Derivatives, Academic Press, New York, 1969.
[52] N.B. Colthup, L.H. Paly, S.E. Wiberley, Introducton to Infrared and Raman Spectroscopy, Academic Press, New York, 1990.
[53] F.R. Dollish, W.G. Fateley, F.F. Bentely, Characteristic Raman Frequencies on Organic Compounds, Wiley, New York, 1997.
[54] D.N. Singh, I.D. Singh, R.A. Yadav, Ind. J. Phys. 76B (3) (2002) 307–318.
[55] R.N. Singh, S.C. Prasad, Spectrochim. Acta A 34 (1974) 39–46.
[56] G. Varsanyi, Assignments of Vibrational Spectra of Seven Hundred Benzene Derivatives, 1/2, Academic Kiaclo, Budapest, 1973.
[57] Y.X. Sun, Q.L. Hao, W.X. Wei, Z.X. Yu, L.D. Lu, X. Wang, Y.S. Wang, J. Mol. Struct.: Theochem. 904 (2009) 74–82.
[58] C. Andraud, T. Brotin, C. Garcia, F. Pelle, P. Goldner, B. Bigot, A. Collet, J. Am. Chem. Soc. 116 (1994) 2094–2102.
[59] V.M. Geskin, C. Lambert, J.L. Bredas, J. Am. Chem. Soc. 125 (2003) 15651–15658.
[60] M. Nakano, H. Fujita, M. Takahata, K. Yamaguchi, J. Am. Chem. Soc. 124 (2002) 9648–9655.
[61] D. Sajan, I.H. Joe, V.S. Jayakumar, J. Zaleski, J. Mol. Struct. 785 (2006) 43–53.
[62] D.A. Kleinman, Phys. Rev. 126 (1962) 1977–1979.
[63] M.C. Ruiz Delgado, V. Hernandez, J. Casado, J.T. Lopez Navarre, J.M. Raimundo, P. Blanchard, J. Roncali, J. Mol. Struct. 651–653 (2003) 151–158.
[64] J.P. Abraham, D. Sajan, V. Shettigar, S.M. Dharmaprakash, I. Nemec, I.H. Joe, V.S. Jayakumar, J. Mol. Struct. 917 (2009) 27–36.
[65] H.O. Kalinowski, S. Berger, S. Braun, Carbon-^{13}NMR spectroscopy, John Wiley & Sons, Chichester, 1988.
[66] K. Pihlaja, E. Kleinpeter (Eds.), Carbon-13 Chemical Shifts in Structural and Sterochemical Analysis, VCH Publishers, Deerfield Beach, 1994.
[67] T.A. Koopmans, Physica 1 (1933) 104–113.